PERGAMON

International Journal of Solids and Structures 40 (2003) 3137–3155

INTERNATIONAL JOURNAL OF SOLIDS and STRUCTURES

www.elsevier.com/locate/ijsolstr

On the axisymmetric progressive crushing of circular tubes under axial compression

F.C. Bardi, H.D. Yun, S. Kyriakides *

Research Center for Mechanics of Solids, Structures and Materials, The University of Texas at Austin, WRW 110, Austin, TX 78712, USA

Received 22 December 2001; received in revised form 5 February 2003

Abstract

Moderately thick circular tubes under compression crush progressively by axisymmetric folding. The paper presents a combined experimental analytical study of the onset of collapse, its localization and the subsequent progressive folding. Results from four displacement controlled crushing experiments are presented on tubes of various radius-to-thickness ratios made of different metal alloys. The experimental results include the crushing response, careful measurements of the geometric characteristics of the folds and the mechanical properties of the alloys. A finite element model of the crushing process has been developed and results from simulations are directly compared with the experiments. The model is found to reproduce the crushing response to a significant degree of accuracy. The mean crushing load is essentially the same as in the experiments; the calculated wavelength of the folds are within a few percent from measured values as are other geometric variables considered. Thus, the crushing energy per unit length of tube is predicted to a very good accuracy. In addition, the model was used to demonstrate that changes in the loading cycles which take place as the number of folds increases, are due to small differences between the inner and outer folds which in turn affect the self contact of the fold walls. Three simpler models taken from the literature in which steady-state folding is modeled by kinematically admissible collapse mechanisms are critically reviewed by comparing predictions of key variables to measured values.
© 2003 Elsevier Science Ltd. All rights reserved.

Keywords: Progressive crushing; Metal tubes; Axial compression

1. Introduction

The axial crushing of thin-walled tubes constitutes a very effective means of absorbing energy. As a result, tubes or assemblages of tubes (e.g. honeycombs with tubular cells of various cross-sections) are widely used in impact mitigation. The simplest problem in the family is the classical axisymmetric progressive collapse exhibited by moderately thin metal tubes. Under axial compression plastic buckling results in localized deformation in the form of one axisymmetric lobe. Subsequently, additional lobes are progressively added

* Corresponding author.
E-mail address: skk@mail.utexas.edu (S. Kyriakides).

0020-7683/03/$ - see front matter © 2003 Elsevier Science Ltd. All rights reserved.
doi:10.1016/S0020-7683(03)00111-2

at a much lower mean load level to form concertina folds (Alexander, 1960; Pugsley and Macaulay, 1960; Horton et al., 1966; Andrews et al., 1983; Allan, 1968). It is this lower mean load level phase of the process which gives such tubes the attractive energy absorption characteristics. As the R/t of a tube increases, initial buckling reverts to a nonaxisymmetric pattern involving circumferential waves (diamond mode, Tvergaard, 1983a). In such tubes, the concertina folds also have increasing number of waves demonstrated clearly in Pugsley and Macaulay (1960), Horton et al. (1966), Andrews et al. (1983) and Allan (1968).

Usually once past the first fold the process is periodic. Over the years most modeling efforts have concentrated on providing estimates of the average load and of the wavelength of steady-state folding. In this study we will revisit the axisymmetric mode of collapse shown in Fig. 1. Alexander (1960) was the first to propose a simple, kinematically admissible collapse mechanism. He assumed the material to be perfectly plastic and calculated approximately the energy required (bending and stretching) for one fold to develop. He equated this with the work done by the average load. The wavelength of the fold was then selected such that the calculated mean load ($\overline{P}$) is minimized. The model was meant as a first approximation and as such the predicted load and wavelength are generally low. Many efforts for improving the predicted results have been made (e.g. Abramowicz and Jones, 1986; Calladine, 1986; Grzebieta, 1990; Wierzbicki et al., 1992; Singace et al., 1995) where more representative kinematical or constitutive models were introduced while the main assumptions of Alexander's model were maintained (i.e., perfect plasticity, infinitesimal deformations, energy balance, minimization of $\overline{P}$ with respect to the wavelength). The two strongest represen-

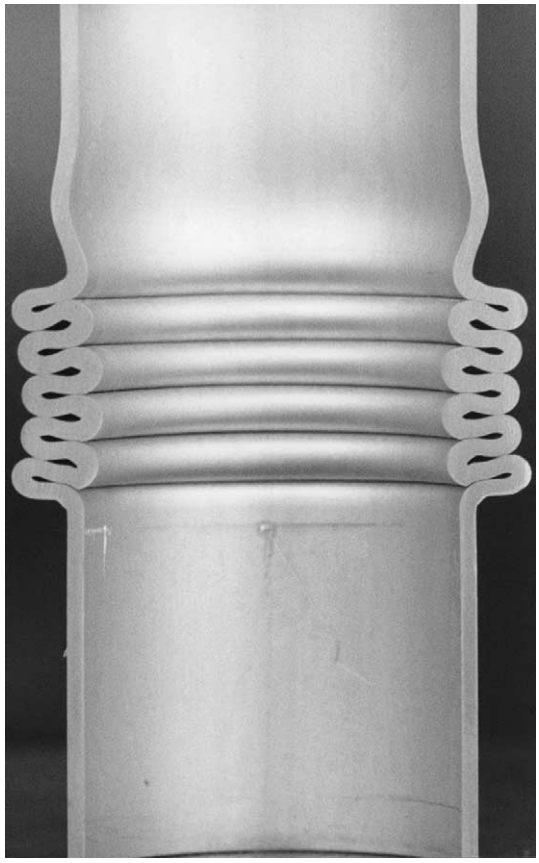

Fig. 1. Cross section of a tube with five axisymmetric folds.

tatives of these (Wierzbicki et al., 1992; Singace et al., 1995) will be discussed and evaluated by comparison to experimental results. An alternative approach where the problem is solved more completely numerically (FE) was presented in Mikkelsen (1999). The results appear to be qualitatively good but quantitative comparison with experiments was not attempted.

Despite its more than 40-year history, the problem remains challenging even for today's numerical tools. The deformation history is complex, it involves large plastic deformations including load reversals, sharp radii of curvature, contact and other challenges. Experimentally the recorded response is influenced by end conditions, load eccentricities and other factors which can distort the periodicity of steady-state folding. Such distortions, which can be seen in many of the responses reported in the literature (e.g. Andrews et al., 1983; Allan, 1968; Grzebieta, 1990; Singace et al., 1995; Singace and Elsobky, 1996), make model evaluation difficult. The objective of this study was to first conduct a series of carefully carried out crushing experiments in which all the relevant variables are established. In the experiments the tube diameter, thickness and material properties were sufficiently varied to establish trends of the effect of these variables on the results. Subsequently, the experiments are simulated with a FE model and the results are critically compared to the measurements. In addition, the performance of the simple model of Alexander and those from two more advanced models (Wierzbicki et al., 1992; Singace et al., 1995) is evaluated by comparing their predictions to the experimental results.

2. Experimental

A series of quasi-static crushing experiments was conducted on tubes of different materials and various R/t values (see Bardi, 2002). Here we will present results from four representative experiments. Two were Al-6061-T6, one carbon steel 1020 and the fourth Al-6260-T4. The three aluminum tubes were seamless whereas the steel one was seam welded. Table 1 lists the main geometric and material parameters of the four tubes. R and t are respectively the average values of several measurements of the mean radius and the wall thickness; L is the overall length of the specimen and N is the number of crushing folds. The stress–strain responses of the materials were measured in uniaxial tension tests using axial strips cut from the tubes. σ_o is the yield stress (stress at a strain offset of 0.2%) and $\bar{\sigma}_o$ is the mean level of stress under the uniaxial stress–strain response (from the yield point up to failure).

The crushing experiments were conducted in a standard servohydraulic testing machine under displacement control. For most experiments reported in the literature the tubes were crushed between parallel rigid plates. Several of the present experiments were conducted in this manner where it was observed that the first fold often was not totally axisymmetric (e.g. part of the edge folded inwards and part outwards). This results in some eccentricity in loading and subsequent distortion of the loading histories of the periodic

Table 1
Geometric and material parameters of tubes tested

Exp. no.	Material	R, in. (mm)	t, in. (mm)	R/t	L/R	E, msi (GPa)	σ_o, ksi (MPa)	$\bar{\sigma}_o$, ksi (MPa)	$\overline{P}$, kips (kN)	$\overline{P}\|_{2-3}$, kips (kN)	N
CR8	Al-6061-T6	0.6015 (15.28)	0.0494 (1.26)	12.18	12.4	10.1 (69.7)	43.62 (300.8)	46.41 (320.1)	4.938 (21.97)	4.942 (21.98)	4
CR10	Al-6061-T6	0.5938 (15.08)	0.0655 (1.66)	9.07	11.7	9.97 (68.7)	37.40 (257.9)	42.65 (293.1)	7.640 (33.99)	7.581 (33.72)	3
CR19	Al-6260-T4	1.1394 (28.94)	0.0804 (2.04)	14.17	8.24	9.2 (63.4)	18.56 (128)	29.06 (200.4)	9.579 (42.61)	9.067 (40.33)	4
CR21	CS-1020	0.6028 (15.31)	0.0498 (1.26)	12.10	11.3	29.45 (203.1)	78.02 (537.9)	89.58 (617.6)	9.539 (42.43)	9.424 (41.92)	6

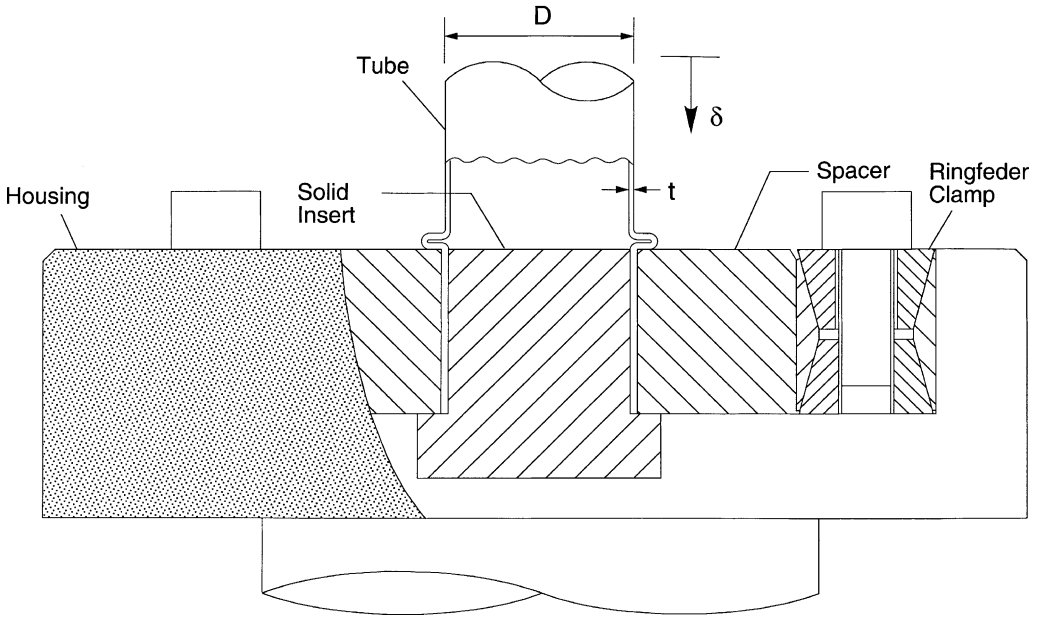

Fig. 2. Experimental setup used to crush tubes under displacement control.

folding. For this reason in the majority of our experiments, including those that will be discussed here, the ends of the tubes were clamped using the custom end fixture shown in Fig. 2.

Close fitting solid inserts are placed inside the ends of the tubes over a length of 1.125 in. (28.6 mm). The outer surface of the tube is in contact with close fitting spacers cut into three sectors. The gap between the sectors enables tightening of the assembly by expanding the *Ringfeder* clamp around it. The outer circumference of the Ringfeder is in contact with a solid steel housing as shown in the figure. In this arrangement the first lobe folds over the solid spacer.

The crushing was conducted at displacement rates that correspond to an average strain rate of about 10^{-2} s^{-1}. Of course, once the deformation localizes the local strain rate increases quite significantly. Furthermore, the strain rate varies at different points of a typical fold with the points at the crowns of the extrados and the intrados experiencing the highest deformation rate. During the experiment, the load (P) and axial deflection (δ) were recorded using a digital data acquisition system. The side of the tube undergoing folding was monitored by a video system run synchronously with the data acquisition system. After the test, it was possible to analyze the events by comparing the force history with the video recording.

We will use results recorded for an Al-6061-T6 tube with $R/t = 12.13$ (CR8 in Tables 1 and 2) to describe a typical sequence of events. Fig. 3 shows the recorded force–displacement response. The load is normalized by the yield load (P_o) and the displacement by the tube radius. Fig. 4 shows a sequence of photographs of the initial stages of the crushing which correspond to the points on the response marked with numbered flags. Initially the tube deforms uniformly. The response is at first elastic and stiff but softens as the tube material plasticizes. The restraints of the clamped edges cause the usual "boundary layer" lobes to form at the ends while the rest of the tube shows signs of axisymmetric plastic buckling (see Batterman, 1965; Batterman and Lee, 1966; Tvergaard, 1983b; Yun and Kyriakides, 1990). At some stage the load reaches a maximum and one of the two end-lobes (in this case the one at the bottom) starts to collapse accompanied by a precipitous drop in the load. The load continues to drop until one side of the first fold which now has a $\subset$-shape (see ①) contacts the solid clamp insert. This stiffens the response temporarily but it reverts to its

Table 2
Comparison of measured and calculated problem variables

Exp. no.		$\overline{P}$, kips (kN)	λ/R	τ_i/t	τ_o/t	r_i/R	r_o/R	ρ_i, in. (mm)	ρ_o, in. (mm)	m
CR8	Experimental	4.939 (21.97)	0.4676	1.279	1.130	0.871	1.267	0.0700 (1.78)	0.0627 (1.59)	0.68
	Numerical	4.950 (22.02)	0.4920	1.164	1.038	0.873	1.292	0.0705 (1.79)	0.0621 (1.58)	0.70
	Alexander	3.553 (15.80)	0.3862	–	–	0.959	1.427	–	–	1
	Wierzbicki et al.	4.435 (19.73)	0.5310	–	–	0.838	1.298	0.0610 (1.55)	0.0610 (1.55)	(0.68)
	Singace et al.	3.271 (14.55)	0.3592	–	–	0.833	1.275	–	–	0.65
CR10	Experimental	7.640 (33.98)	0.6106	1.353	1.142	0.859	1.352	0.0882 (2.24)	0.0790 (2.01)	0.71
	Numerical	7.710 (34.30)	0.6316	1.231	1.063	0.839	1.364	0.0916 (2.33)	0.0802 (2.04)	0.69
	Alexander	4.999 (22.24)	0.4476	–	–	0.945	1.503	–	–	1
	Wierzbicki et al.	6.182 (27.50)	0.6154	–	–	0.818	1.367	0.0697 (1.77)	0.0697 (1.77)	(0.71)
	Singace et al.	4.595 (20.44)	0.4162	–	–	0.799	1.326	–	–	0.65
CR19	Experimental	9.576 (42.60)	0.4278	1.279	1.130	0.894	1.267	0.1215 (3.09)	0.1073 (2.73)	0.72
	Numerical	9.261 (41.19)	0.4626	1.149	1.009	0.886	1.274	0.1241 (3.15)	0.1110 (2.82)	0.71
	Alexander	6.331 (28.16)	0.3580	–	–	0.965	1.393	–	–	1
	Wierzbicki et al.	7.935 (35.30)	0.4922	–	–	0.866	1.288	0.1070 (2.72)	0.1070 (2.72)	(0.72)
	Singace et al.	5.832 (25.94)	0.3330	–	–	0.848	1.252	–	–	0.65
CR21	Experimental	9.539 (42.43)	0.4314	1.354	1.140	0.896	1.282	0.0693 (1.76)	0.0613 (1.56)	0.72
	Numerical	9.586 (42.64)	0.4380	1.291	1.143	0.869	1.251	0.0675 (1.71)	0.0592 (1.50)	0.66
	Alexander	6.950 (30.92)	0.3874	–	–	0.959	1.429	–	–	1
	Wierzbicki et al.	8.673 (38.58)	0.5326	–	–	0.853	1.314	0.0613 (1.56)	0.0613 (1.56)	(0.72)
	Singace et al.	6.398 (28.46)	0.3602	–	–	0.833	1.275	–	–	0.65

downward path soon thereafter (②) when the ⊂-shape continues its collapse. Collapse is arrested when the walls of the ⊂ come into contact and the load starts to increase once more. This first fold is slightly different from subsequent ones due to the flat constraint provided by the rigid clamp. In configuration ③, a new outward fold is seen to form. Eventually a second local load maximum develops and the second fold starts to collapse as seen in ④. The load starts to recover once more when the outer knee comes into contact with the first fold (⑤ occurs soon after contact). The load rises until an inward lobe starts to form and to collapse (near ⑥). Eventually the walls of the inner lobe come into contact (see ⑦) completing one steady-state

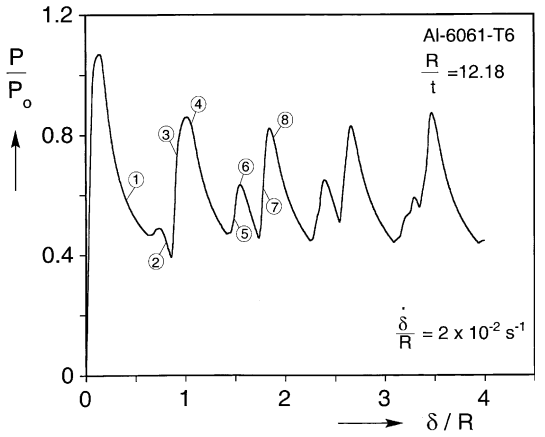

Fig. 3. Measured force–displacement response for tube CR8.

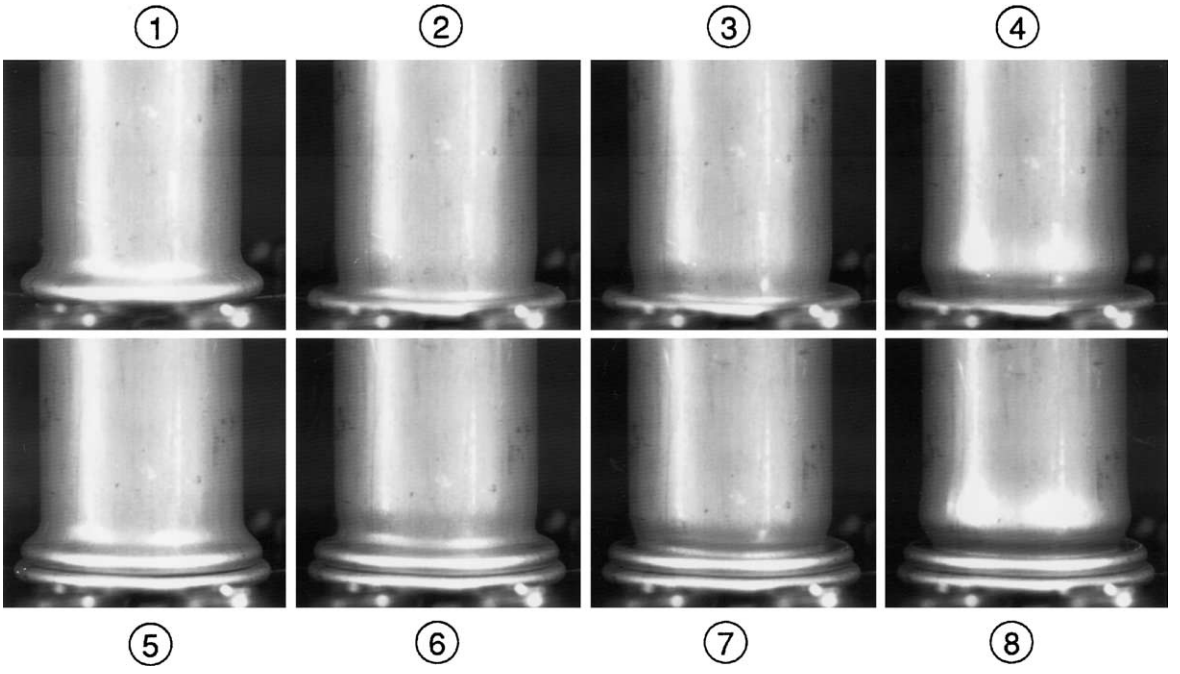

Fig. 4. Sequence of configurations illustrating progressive crushing of a tube (correspond to points identified with numbered flags on response in Fig. 3).

period of folding. A new fold starts to occur at the next local maximum and a second folding period consisting of a high and a low stress peak starts to develop.

The second folding period is similar to the first one. The two stress peaks and valleys are at about the same levels and their extent is also approximately the same. The first half of the third period is also similar but the second stress valley is somewhat higher while simultaneously the folding started showing signs of

loss of axial symmetry where one side would fold a bit earlier than the other. By the fourth cycle the lower stress peak has almost disappeared. This tendency for distortion after 3–5 cycles was observed in all the experiments. The tubes tested were kept at relatively short lengths ($4 < L/D < 6$) in order to avoid other forms of buckling. Thus, after the first few folds had formed, the length of undeformed tube left became relatively short and this added some constraint to the folding process. Also, our setup is such that some small eccentricity between the upper grip and the lower one is unavoidable. This eccentricity is accentuated as the grips come closer together resulting in the gradual loss of axial symmetry. An additional contributing factor is that the inner radius and thickness of each fold are larger than the corresponding values of the outer one. Thus, as additional folds stack up they become inclined which affects the time contact takes place (this will be further discussed later with the help of analytical results).

The mean load $\overline{P}$ for the whole history is listed in Tables 1 and 2. Also listed in Table 1 is the mean load of two steady-state periods (usually the second and third folds $\overline{P}|_{2-3}$).

2.1. Dimensional measurement of crushed tubes

After each experiment, the deformed inner and outer radii of the folds r_o and r_i defined in Fig. 5, were measured and are reported in Table 2. The values give a clear indication of the magnitude of the circumferential strain. For example, for CR10 the circumferential strain of the crown of the extrados is more than 28%. The variable m represents the ratio

$$m = \frac{r_o - R}{r_o - r_i}. \tag{1}$$

The tubes were then sectioned into two halves and the surfaces of the cuts were polished and photographed (e.g. see Fig. 1). The photographs were digitized and the NIH image processing system was used to perform the following additional measurements. The deformed thickness at the outer and inner crests of each fold, τ_o and τ_i defined in Fig. 5, were measured and average values for each are listed in Table 2. The inner and outer crests of each fold were fitted with circular arcs which approximately represent the radii of

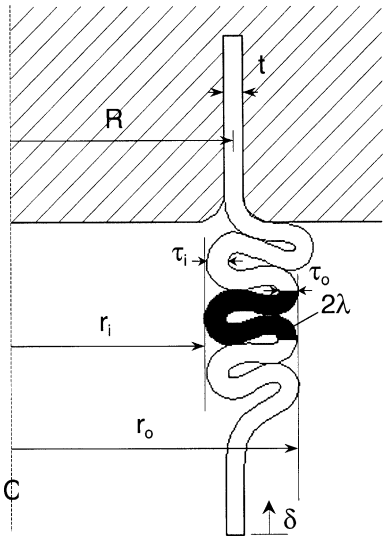

Fig. 5. Definition of problem geometric parameters.

curvature ρ_i and ρ_o listed in Table 2. Once more, the change in thickness as well as the sharpness of the radii give an indication of the very significant deformation induced by folding. For example, the thickness at the crest of the inner fold (τ_i) in CR10 changed by about 35%. It should be noted however, that both the thickness and radii of curvatures selected are difficult to measure accurately (see Bardi, 2002). Thus the results are quoted mainly for qualitative purposes.

Because the material inside the folds undergoes finite deformations, the wavelength (2λ) was calculated using undeformed measures of length as follows. Before each experiment, the tube surface was coated with a thin layer of red layout ink. Circumferential lines were then scratched at intervals of 0.050 in. (1.27 mm). After each experiment the video recording was analyzed and the wavelength of each fold was determined by counting the number of lines between the ridges of adjacent folds. The count had to be made as the folding progressed and before contact between the folds developed. The wavelength of at least two folds was measured in this manner and the values reported in Table 2 represent the average of each set of measurements. The accuracy of the reported value of 2λ is of the order of one-quarter of the spacing of the marker lines.

Results from four experiments are listed in Tables 1 and 2. They represent various R/t values, and materials of different moduli, yield stresses and hardening characteristics (the latter is represented by the difference between σ_o and $\bar{\sigma}_o$).

3. Analysis

The problem will be analyzed first using existing plastic hinge models. Three such models will be evaluated by direct comparison of their predictions with the experiments. The main effort of the present study involves a finite element model which will be similarly evaluated against the experimental results.

3.1. Plastic hinge models

A significant body of work exists in which kinematically admissible mechanisms coupled with perfect plasticity were used to predict steady-state axisymmetric collapse (Abramowicz and Jones, 1984, 1986; Calladine, 1986; Grzebieta, 1990; Wierzbicki et al., 1992; Singace et al., 1995). In such models, the bending and stretching energy of folding is estimated from the mechanism assumed and equated with the work done by the mean applied axial force ($\overline{P}$). The models also assume infinitesimal deformations, neglect interaction between membrane and bending stresses as well as any effects due to reverse loading. The wavelength (2λ) and, in some cases additional parameters such as m, are then chosen in a manner that minimizes $\overline{P}$.

We will consider three such models in which the mechanisms assumed are of increasing complexity and, as a result, are increasingly more representative of reality. Each model will be used to predict the mean load of each of the four experiments discussed in the previous section and as many of the geometric variables of interest as possible. The models do not account for strain hardening so to correct this to the extent possible, the "yield stress" that will be adopted is the mean value of stress under the measured stress–strain response between the yield point and failure in a uniaxial test ($\bar{\sigma}_o$ in Table 1).

3.1.1. Alexander (1960)

The folding mechanism assumed in this first attempt at the problem is shown in Fig. 6. It is a crude approximation of the actual behavior seen in Fig. 1 as it does not include the curvature of the folds and neglects the fact that the tube folds partly inwards and partly outwards from the original tube mid-surface. Because of these differences, the two-peak and two-valley character of each folding period is missed. The differences also have implications on the deformation history seen by different points along the fold. Expressions for the mean load $\overline{P}$ and the half wavelength λ are given in Appendix A. The predictions of these

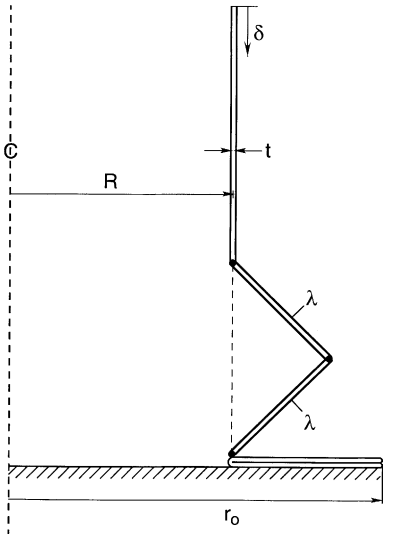

Fig. 6. Alexander's crushing mechanism.

variables for the four tubes tested are listed in Table 2. The predicted values of $\overline{P}$ range from 65 to 73% of the measured values. The predicted values of λ range from 73 to 90% of the measured values. A modification of this model which appeared in Abramowicz and Jones (1984) improves somewhat the predicted mean load but lowers further the predicted values of λ.

3.1.2. Singace et al. (1995)

An improvement on this linear segment folding mechanism, which allows for partial folding inside and outside the original mid-surface shown in Fig. 7, was proposed by Wierzbicki et al. (1992). The ratio m was left undefined which prompted an extension by Singace et al. (1995). This extension yielded a fixed value of $m = 0.65$ and the values for the remaining key variables given in Appendix A. The predictions for the four tubes tested appear in Table 2. Interestingly, the predicted mean loads are somewhat lower than those predicted by Alexander's model and, as a result, worse in comparison to the experimental values (range 60–67% of measured $\overline{P}$). The values of the wavelengths are also lower than those of Alexander's as they range between 68% and 83% of the measured values. It should be pointed out that the minimization of $\overline{P}$ with respect to both m and λ is based on a postulate and not on a law of mechanics. As in other similar problems, application of this postulate, often leads to inaccurate predictions of key problem variables (see similar observations on this issue made by Calladine, 1986).

3.1.3. Wierzbicki et al. (1992)

A more realistic concertina folding mechanism proposed in Wierzbicki et al. (1992) is shown in Fig. 8. Here the folds consist of circular arcs of constant radius ρ. The model also allows partial folding inside and outside the original mid-surface, but the ratio m is not defined. The resultant expressions for the key problem variables are given in Appendix A. Predicted values of these variables for the four tubes tested are listed in Table 2. While $\overline{P}$ is independent of m, its predicted values are in the range of 81–91% of the measured values. Thus, these predictions are approaching acceptable engineering accuracy. The biggest difference with the experiments occurs for CR10 and CR19. The first is a low R/t tube which undergoes the largest deformations which are not accounted by the model. CR19 exhibited a stress–strain behavior with high strain hardening. For this case, the comparison of the predicted $\overline{P}$ with experiment is more favorable if

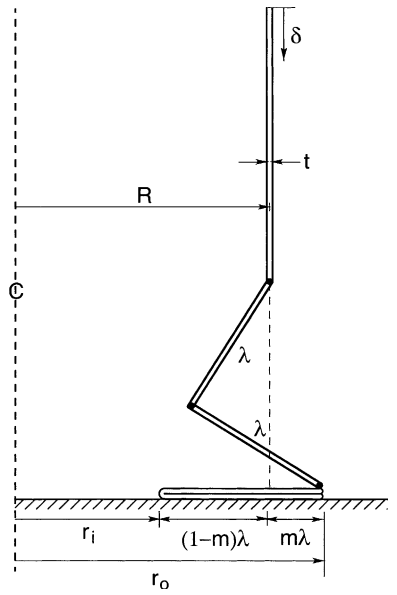

Fig. 7. Singace et al.'s crushing mechanism.

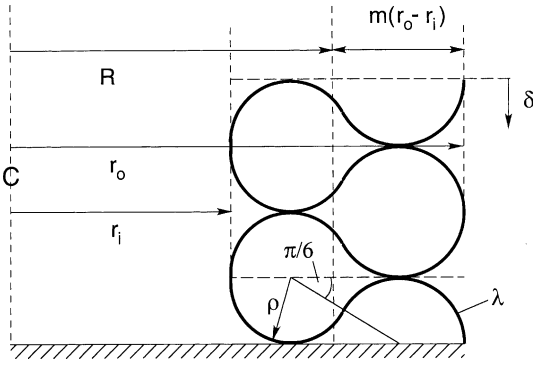

Fig. 8. Wierzbicki et al.'s crushing mechanism.

$\overline{P}|_{2-3}$ from Table 1 is used instead. The folding ratio m which is a free variable in this model affects several of the geometric variables through Eq. (1). In order to place the model in the best possible light, the value of m measured in each experiment was used when calculating the affected variables. The predicted wavelengths are higher than the measured values by values of 1–23%.

In Table 2 predictions for r_i, r_o and ρ are listed. The values appearing in the original reference are based on mid-surface coordinates. In order to make the comparison with the measurements more realistic the values quoted for r_i and r_o include a correction by $t/2$ for each of these variables (using the undeformed measure of t). The model predicts a single value for ρ, whereas the experiments show a difference between the inside and outside folds. Furthermore, ρ_i and ρ_o were measured on the extreme fibers of each fold. Thus, any comparison with the predicted values of ρ is of qualitative nature.

In summary, the first two kinematically admissible crushing mechanisms yielded predictions for $\overline{P}$ which can be considered of qualitative value. The third model, with its more realistic crushing mechanism, yielded predictions which can be considered of engineering accuracy. The predictions of the wavelength of the folds was generally poor for all three models. This is a weakness because it implies that the predicted crushing energy per unit undeformed length of tube, a variable of significant practical interest, can differ significantly from measured values.

3.2. Numerical model

As we have seen, the problem is characterized by finite plastic deformations, sharp changes of curvature, and contact (on both sides of each fold). A finite element model capable of handling these nonlinearities was developed within the code ABAQUS (6.1). The geometry used for most calculations performed is shown in Fig. 9. It resembles the geometry of the experimental setup. The tube has an initial mid-surface radius R and wall thickness t. One end is held in a rigid clamp to a depth a. The outer part of the clamp can be moved radially to provide an initial clamping stress on the constrained length. The entrance to the clamp is radiused (r_c) to resemble the actual clamps. Unless otherwise stated and without loss of generality the deformation is assumed to be symmetric about the mid-height of the tube and thus only one half of the length was modeled. The value of the length (L) used corresponds to that of each experiment listed in Table 1.

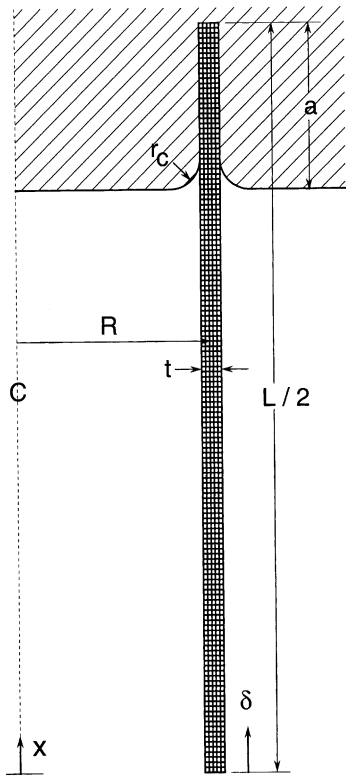

Fig. 9. Initial geometry of axisymmetric model.

The domain is discretized with four-noded, linear, axisymmetric elements with reduced integration and hourglass control (CAX4R—one integration point). Through convergence studies it was established that five elements through the thickness with an axial-to-width aspect ratio of 5:4 were sufficient. This results in a relatively high density of elements in the axial direction which is necessary because of the very tight curvatures of the folds (see Fig. 1). Contact between the rigid clamp and the tube was treated by defining two master/slave contact pairs. The masters being the inner and outer parts of the clamp and the slave the surface of the tube. Contact between the folds was treated via the self-contact option of the code for axisymmetric models.

The material was modeled as a time-independent, finitely deforming, elastic–plastic solid which hardens isotropically. In each case the model was calibrated using the true stress–logarithmic strain version of the measured uniaxial stress–strain response. In all cases the uniaxial test specimens failed at strain levels which were smaller than the strains experienced at the most deformed parts of the crushed structure. For example Fig. 10 shows an engineering stress–strain response typical of the typical Al-6061-T6 alloys used. This specimen failed at just under 12% strain. In view of this limitation the measured true stress–logarithmic strain responses were linearly extrapolated so that a continuous constant slope was maintained with the termination of the measured part.

The clamping of the end was simulated numerically by moving the outer clamp until a stress corresponding to 50% of the material yield stress was reached. This was done with the specimen free axially. Subsequently, the position of the clamps was fixed and the tube was compressed by prescribing the axial displacement δ of the symmetry plane (see Fig. 9). The total force acting on the end of the tube on the symmetry plane was evaluated from the stresses at the nodes.

Fig. 11 shows the calculated force–displacement response for tube CR8. Its major characteristics are similar to those of the experimental response. Fig. 12 shows a set of deformed configurations of an axial section corresponding to the peaks and valleys of the response marked with numbered flags. The first eight of these can be compared approximately to the deformed configurations from the video recording of the experiment in Fig. 4. Initially, the response is elastic and stiff. Because of the end constraint the tube develops a local buckle close to the edge discernable in configuration ① which corresponds to the first load maximum (onset of collapse). The buckle collapses into a ⊂-shape. When the upper wall of this shape comes into contact with the rigid clamp (②), collapse is temporarily halted resulting in the small stress peak corresponding to ③. This is a short lived event as, after ③, collapse continues with the formation of an inward fold. Collapse is arrested for good when the inner walls of the ⊂-shape come into contact at ④. The load then rises to a new local maximum which occurs at ⑤ when a new outward fold starts to form. The first half of the new folding is completed by ⑥ when the outer knee formed comes into contact with the first fold. The load increases once more until at ⑦ an inward fold starts to form while the load drops once more.

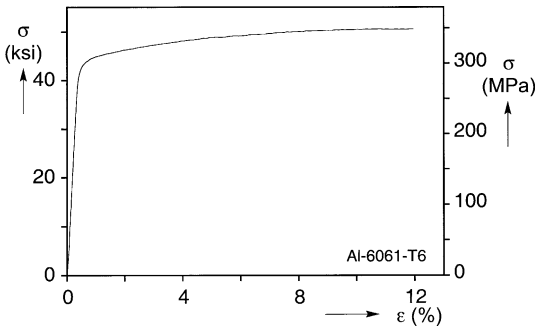

Fig. 10. Measured stress–strain response typical of the Al-6061-T6 alloys used in the crushing experiments.

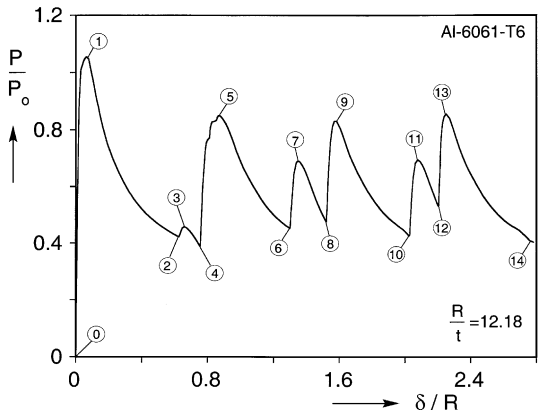

Fig. 11. Calculated force–end displacement response for tube CR8.

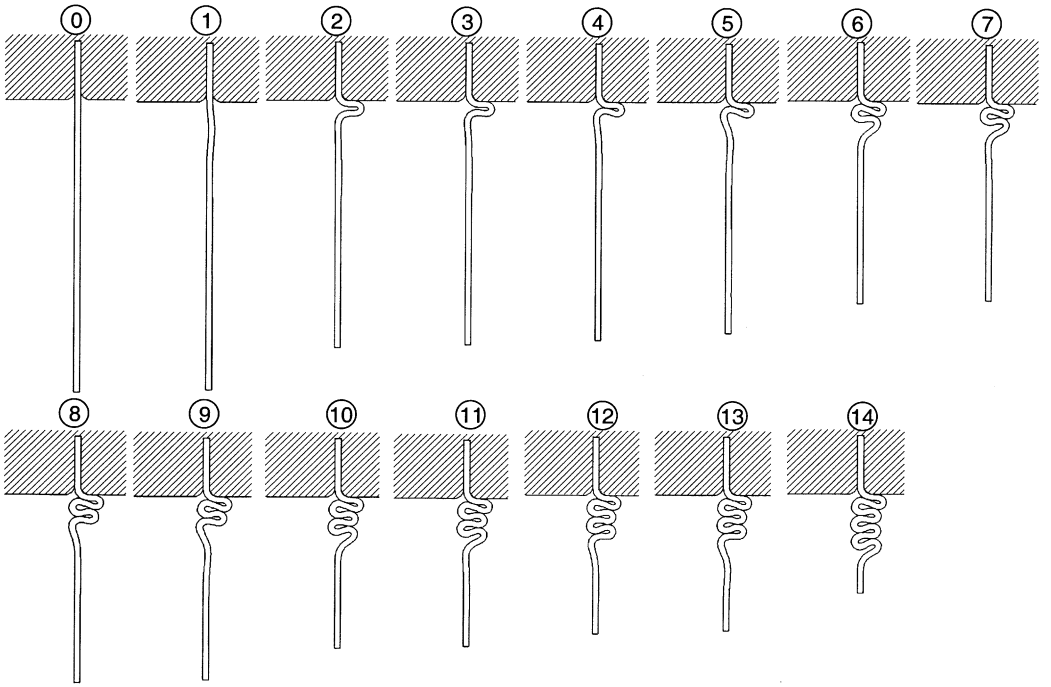

Fig. 12. Sequence of calculated deformed configurations showing the progressive crushing of tube CR8 (correspond to numbered points in Fig. 11).

At ⑧ collapse of this fold is arrested by contact, completing one steady-state folding cycle (④–⑧). The next cycle (⑧–⑫) is almost identical to this one consisting again of two load peaks and two valleys corresponding to the onset of folding outside and inside and contact between the walls of the folds at the inner and outer sites. The second valley is at a somewhat higher load level indicating a change which will be discussed below.

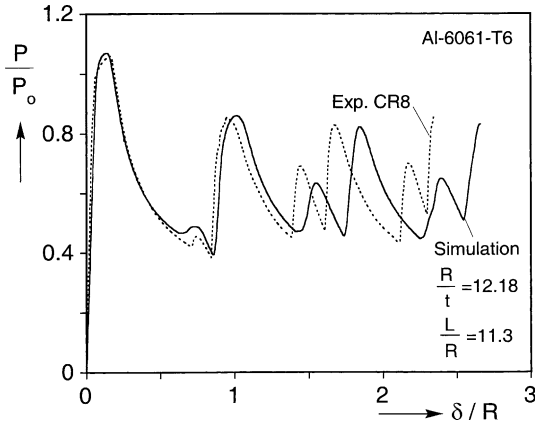

Fig. 13. Comparison of measured and calculated load-deflection response for tube CR8.

The simulated response is compared directly with the experimental one of tube CR8 in Fig. 13. We note that in this case, in order to get better agreement between experiment and analysis in the early part of the response representing the onset of collapse, the length analyzed was the same as the length of the actual tube tested given in Table 1. The onset of collapse is seen to be predicted quite accurately. The depth of the first load valley is accurate while the small load peak that precedes it is slightly smaller than the experimental one. This part of the response is affected by the length of the test specimen. Accurate prediction of the response requires accurate modeling of the details of the clamped part of the tube. The next two load peaks and valleys are also reproduced with accuracy and so are the subsequent ones. The main difference between the two responses is in the wavelength of the periodic crushing. The wavelength is slightly larger in the simulation and this results in the progressive shifting between the two responses seen in Fig. 13. The amplitude of the small load undulation near the first load valley and that of the smaller load peak of subsequent cycles was found to be influenced by details such as the radius r_c of the corners of the clamps (see Fig. 9). This affects the shape of the first fold which in turn affects to some degree when contact takes place in subsequent cycles.

The wavelength 2λ was calculated, in undeformed measure of length, from the simulation by back tracking the coordinates of the inner and outer ridges of the folds to the undeformed configuration. This scheme is similar to that used to measure 2λ in the experiment except that here the accuracy of the measurement is much higher because of the high density of elements in the axial direction (47 in one wavelength for CR8). The calculated half wavelength is $\lambda = 0.492R$ which is 5.2% higher than the measured value. However, this value is much closer to the experiment than wavelengths listed in Table 2 from the simpler models. The calculated mean load $\overline{P} = 4950$ lb (22.02 kN) is just 0.22% higher than the measured value. Again, this level of accuracy is far superior to the predictions from the simple models.

The remaining geometric characteristics of the folds $(\tau, r, \rho)_{i,o}$ and m were measured from the simulation using essentially the same procedures as in the experiments and the results are listed in Table 2. The values of the deformed wall thicknesses at the crests of the folds $\tau_{i,o}$ are seen to be somewhat smaller than the measured values. The radii of the inner and outer folds $r_{i,o}$ match the measured values well; the folding ratio parameter $m = 0.70$ which compares with the measured value of 0.68. Finally, the radii of curvature of the intrados and extrados $\rho_{i,o}$ are in good agreement with the experimental values.

Despite the small differences between the predicted and measured values of the geometric variables (λ, τ, r, ρ), the simulation overall is of very high accuracy. This includes the crushing energy per unit length of the tube which is within 5% of the measured value. The small differences in the geometric values are attributed first to the constitutive model adopted and to uncertainty introduced by the linear extrapolation of the

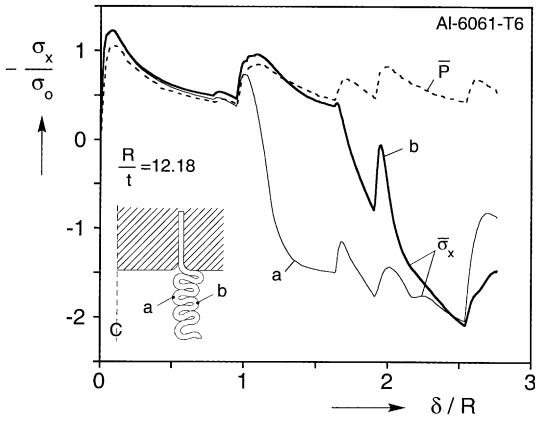

Fig. 14. Axial stress histories at an extrado and an intrado for tube CR8.

measured uniaxial stress–strain responses. The first point is illustrated in Fig. 14 which shows the true-axial stress histories (as a function of the axial displacement) calculated for points *a* and *b* identified in the inset. Included is also the overall axial load history ($\overline{P}$). Initially $\bar{\sigma}_a$ and $\bar{\sigma}_b$ follow the overall load history as they are away from the site of the first buckling lobe. The points undergo net compression which takes them into the plastic range. Soon after the formation of the first fold, point *a* undergoes reverse loading which takes it to very significant tensile stress levels resulting from the high bending strains. Point *b* is one half a cycle behind point *a* and, as a result, its stress reversal is delayed until soon after the second overall load valley. Both points experience some cycling in stress which correspond to the cycles of $\overline{P}$. Isotropic hardening is not an ideal model for loading histories which experience severe load reversals. Use of this model generally makes the material less compliant. In this particular case the first excursion into the plastic range was limited. As a result this effect played a smaller role and resulted in the excellent prediction of the crushing history.

The effect of the extrapolation of the measured stress–strain response was studied by varying the slope of the extrapolated part. Increasing/decreasing the slope of the linear extrapolation was found to respectively increase/decrease the period of the cycles, the deformed thickness variables $\tau_{i,o}$ and the radii $\rho_{i,o}$ of the folds. This change only had a minor effect on the mean load $\overline{P}$ as it only affected slightly the height of the lower stress peaks of the cycles.

One other factor that can affect the geometric variables (λ, τ, r, ρ) is the density of the discretization mesh. Inadequate number of elements can make the folds less compliant. The adequacy of the discretization scheme adopted was confirmed through the mesh convergence studies performed (see Bardi, 2002).

We now show the continuation of the simulation of the crushing of tube CR8 beyond the 3rd crushing cycle. The calculated force–displacement response is shown in Fig. 15, while Fig. 16 shows additional deformed configurations corresponding to the numbered load peaks and valleys in Fig. 15. In cycle 4, the intermediate load peak and valley are more distorted and by cycle 5 they have been altogether erased. This degradation in the cycle characteristics is attributed to the following. The deformed thickness and radii of the inner lobes (τ_i, ρ_i) are larger than the corresponding values of the outer lobes (τ_o, ρ_o). This difference implies that the inner folds take more space in the axial direction than the outer ones. This introduces a gradual inclination of the folds. The inclination is seen in Fig. 16 to increase as the number of folds increases. This causes earlier contact for the inner fold and delayed contact for the outer fold. In configurations ⑤ and ⑥ the contact of the inner and outer folds is seen to be almost simultaneous. As a consequence, the intermediate part of the cycle has been erased completely.

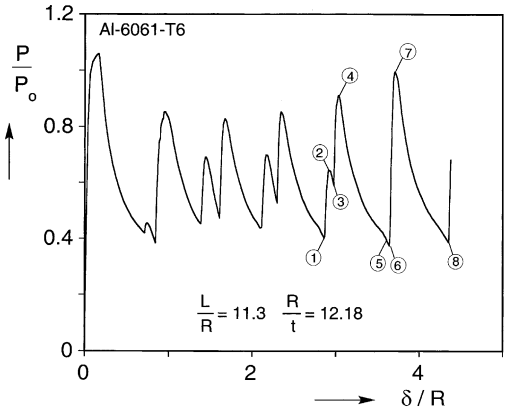

Fig. 15. Calculated force–displacement response for tube CR8 showing progressive degradation of load cycle characteristics.

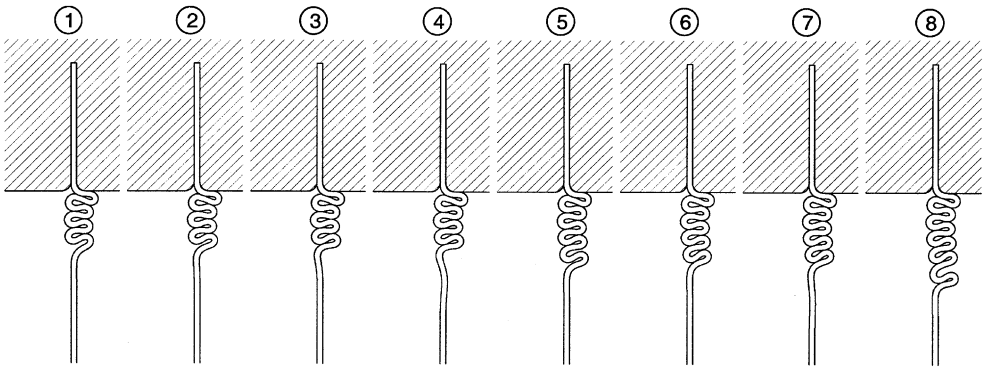

Fig. 16. Calculated deformed configurations showing progressive increase in inclination of folds (correspond to numbered points in Fig. 15).

The geometry of the first fold which, as mentioned above, is sensitive to the radius r_c of the clamps, tends to affect the orientation of subsequent folds in a similar way and also affects the evolution of the intermediate load peaks. Interestingly neither factor was found to affect the overall wavelength of the cycles. This variable is not dependent on the details of the contact of the folds but is instead a function of the tube geometry R/t and its stress–strain characteristics. All observations made here relating to changes in the loading cycle including the timing of the onset of the changes, correspond very well to experimental events discussed earlier.

The results from the numerical simulations for the remaining three tubes analyzed are summarized in Table 2. The average crushing load $\overline{P}$ compares very well with the measured values. The biggest difference is −3.3% for tube CR19. For tubes CR10 and CR21, the wavelengths of the folds match well the measured values. For CR19 the wavelength is 8.1% higher than the experimental value. This particular aluminum alloy exhibited low yield stress and high hardening. Thus the use of isotropic hardening to model the material plasticity results in more error than in the other cases.

The calculated values of (τ_o, τ_i) are lower than the experimental values for CR10 and CR19 and quite good for CR21. The radii of the inner and outer folds (r_o, r_i) and the variable m are in very good agreement

with the experimental values for all four cases. The radii of curvature of the folds (ρ_o, ρ_i) are also in good agreement with the experimental values. Thus, overall, the predictive capability of the numerical model developed coupled with the constitute model used produce results which are in very good agreement with corresponding experimental results.

4. Conclusions

Moderately thick circular tubes under compression crush progressively by axisymmetric folding. This classical problem has been revisited through a combined experimental/analytical study of the onset of collapse, its localization and of the subsequent progressive folding. Results from four displacement controlled crushing experiments have been presented involving tubes of various radius-to-thickness ratios made of different metal alloys exhibiting various degrees of hardening. A finite element model of the crushing process has been developed and used to directly simulate each experiment. Three simpler models taken from the literature, which involve kinematically admissible collapse mechanisms of increasing complexity, have been critically reviewed by comparing their predictions of key variables to measured values. The following conclusions can be drawn from the study:

(a) Moderately thick-walled tubes collapse axisymmetrically and crush by progressive folding with a well defined period. The transition from axisymmetric to nonaxisymmetric collapse and crushing depends on the tube R/t and on the hardening characteristics of the material. A typical steady-state folding period involves two load peaks and valleys associated with buckling and self-contact of the walls inside and out. Under the testing conditions used, it was found that after a few cycles the steady-state folding reverted to a single load peak and valley due to the way the folds stacked up.

(b) Because axisymmetric crushing occurs for moderately thick-walled tubes, the axial and circumferential strains in the folds are large (~25–50%) and this needs to be addressed in any modeling effort. A finite element crushing model has been developed which suitably models the geometric and contact nonlinearities while representing the material as a finitely deforming, J_2-type, elastoplastic solid which hardens isotropically. The model was found to reproduce very well the onset of collapse, its localization as well as the details of steady-state folding. The changes in the periodic load cycles mentioned above were also captured with accuracy. The mean crushing load was predicted with great accuracy as was the period of the folds. Thus, the energy absorption per unit length of tube is also predicted to very good accuracy.

(c) Some points along the length of the tube experience some loading and reverse loading. Despite this, isotropic hardening plasticity which for materials with healthy hardening does not reproduce accurately reverse loading was found to perform adequately in the four cases analyzed.

(d) The three simpler models considered mainly aimed at predicting the mean crushing load and the period of folding. The models of Alexander and Singace et al. underpredicted the crushing load significantly while the model of Wierzbicki et al. yielded values of engineering accuracy due to the more realistic folding mechanism assumed. The prediction of the period of folding was less successful for all three models.

Appendix A. Summary of predictions from three plastic hinge models

(a) Alexander (1960)

The tube is assumed to collapse in the manner shown in Fig. 6. The half wavelength (λ) of the fold and the mean load of steady-state cycles ($\overline{P}$) were calculated to be

$$\frac{\lambda}{R} = \sqrt{\frac{\pi}{\sqrt{3}}}\left(\frac{t}{R}\right)^{1/2} \cong 1.347\left(\frac{t}{R}\right)^{1/2}, \tag{A.1}$$

$$\overline{P} \cong \bar{\sigma}_o t^2 \left[8.462 \left(\frac{R}{t} \right)^{1/2} + 1.814 \right]. \tag{A.2}$$

(b) Singace et al. (1995)

The tube is assumed to collapse as shown in Fig. 7. The geometric variables are given by

$$\frac{\lambda}{R} = \sqrt{\frac{\pi}{2}} \left(\frac{t}{R} \right)^{1/2} \cong 1.253 \left(\frac{t}{R} \right)^{1/2} \quad \text{and} \quad m = 0.65. \tag{A.3}$$

The mean load of a steady-state cycle depends on m and was calculated to be

$$\overline{P} = \bar{\sigma}_o t^2 \left[7.874 \left(\frac{R}{t} \right)^{1/2} + 1.408 \right]. \tag{A.4}$$

(c) Wierzbicki et al. (1992)

The tube is assumed to collapse as shown in Fig. 8. The geometric variables are given by

$$\rho = \frac{3\lambda}{5\pi}, \quad r_o - r_i = 2\rho \left(1 + \frac{\sqrt{3}}{2} \right) \quad \text{and} \quad \frac{\lambda}{R} \cong 1.853 \left(\frac{t}{R} \right)^{1/2}. \tag{A.5}$$

The ratio of material folding outside to that involved in a fold, m given in Eq. (1), is an undecided variable. The mean load of a steady-state cycle is independent of m and is given by:

$$\overline{P} \cong 11.22 \bar{\sigma}_o t^2 \left(\frac{R}{t} \right)^{1/2}. \tag{A.6}$$

References

Abramowicz, W., Jones, N., 1984. Dynamic axial crushing of circular tubes. International Journal of Impact Engineering 2, 263–281.

Abramowicz, W., Jones, N., 1986. Dynamic progressive buckling of circular and square tubes. International Journal of Impact Engineering 4, 243–270.

Alexander, J.M., 1960. An approximate analysis of the collapse of thin cylindrical shells under axial loading. Quarterly Journal of Mechanics and Applied Mathematics 13, 10–15.

Allan, T., 1968. Experimental and analytical investigation of the behaviour of cylindrical tubes subject to axial compressive forces. Journal of Mechanical Engineering Sciences 10, 182–197.

Andrews, K.R.F., England, G.L., Ghabi, E., 1983. Classification of the axial collapse of cylindrical tubes under quasi-static loading. International Journal of Mechanical Sciences 25, 687–696.

Bardi, F.C., 2002. Progressive crushing of tubular structures. MS Thesis, University of Texas at Austin, MSS&M Report No. 02/06.

Batterman, S.C., 1965. Plastic buckling of axially compressed cylindrical shells. AIAA Journal 3, 316–325.

Batterman, S.C., Lee, L.N.H., 1966. Effects of modes on plastic buckling of compressed cylindrical shells. AIAA Journal 4, 2255–2257.

Calladine, C.R., 1986. Analysis of large plastic deformation in shell structures. In: Bevilacqua, L., Feijoo, R., Valid, R. (Eds.), Inelastic Behaviour of Plates and Shells. Springer, Berlin, Heidelberg.

Grzebieta, R.H., 1990. An alternative method of determining the behaviour of round stocky tubes subjected to an axial crush load. Thin-Walled Structures 9, 61–89.

Horton, W.H., Bailey, S.C., Edwards, A.M., 1966. Nonsymmetric buckle patterns in progressive plastic buckling. Experimental Mechanics 6, 433–444.

Mikkelsen, L.P., 1999. A numerical axisymmetric collapse analysis of viscoplastic cylindrical shells under axial compression. International Journal of Solids and Structures 36, 3269–3288.

Pugsley, A., Macaulay, M., 1960. The large scale crumpling of thin cylindrical columns. Quarterly Journal of Mechanics and Applied Mathematics 13, 1–9.

Singace, A.A., Elsobky, H., 1996. Further experimental investigation on the eccentricity factor in the progressive crushing of tubes. International Journal of Solids and Structures 33, 3517–3538.

Singace, A.A., Elsobky, H., Reddy, T.Y., 1995. On the eccentricity factor in the progressive crushing of tubes. International Journal of Solids and Structures 32, 3589–3602.

Tvergaard, V., 1983a. On the transition from a diamond mode to an axisymmetric mode of collapse in cylindrical shells. International Journal of Solids and Structures 19, 845–856.

Tvergaard, V., 1983b. Plastic buckling of axially compressed circular cylindrical shells. Thin-Walled Structures 1, 139–163.

Wierzbicki, T., Bhat, S.U., Abramowicz, W., Brodkin, D., 1992. Alexander revisited—A two folding elements model of progressive crushing of tubes. International Journal of Solids and Structures 29, 3269–3288.

Yun, H., Kyriakides, S., 1990. On the beam and shell modes of buckling of buried pipelines. International Journal of Soil Dynamics and Earthquake Engineering 9, 179–193.